Applied Clay Science 230 (2022) 106696

Contents lists available at ScienceDirect

Applied Clay Science

journal homepage: www.elsevier.com/locate/clay

Research Paper

Mimicking the cementation mechanism of ancient Roman seawater concrete using calcined clays

Warda Ashraf [a,*], Ishrat Baki Borno [a], Rakibul I. Khan [b], Salman Siddique [a], Muhammad Intesarul Haque [a], Adhora Tahsin [a]

[a] Department of Civil Engineering, University of Texas at Arlington, Nedderman Hall, Arlington, TX 76010, USA
[b] Laticrete International, Inc., Bethany, CT 06524-3423, USA

ARTICLE INFO

Keywords:
Calcined clay
Seawater
Roman concrete
NMR
XRD

ABSTRACT

The negative environmental impacts of Ordinary Portland Cement (OPC)-based materials, including high carbon emission, energy-intensive manufacturing process, and freshwater consumption, can be minimized by capitalizing on the concepts of ancient Roman concrete. Accordingly, this study presents a pathway of producing durable and sustainable seawater concrete by mimicking the cementation of ancient Roman concrete. Calcined clays with blended minerals (kaolinite and montmorillonite), portlandite, and seawater were used to produce these binder mixtures. The evolutions of the reaction products of the seawater-cured paste samples were monitored for up to 56 days using Thermogravimetric analysis (TGA), X-ray diffraction (XRD), Nuclear Magnetic Resonance (NMR), and Scanning Electron Microscopy-Energy Dispersive Spectroscopy (SEM-EDS). Because of the high alkalinity (pH 8.2) of seawater, it acts as an activator for the calcined clay-portlandite mixtures eliminating the need for additional alkali activators. Accordingly, in the presence of seawater, the reaction between calcined clay and portlandite happens relatively rapidly, and compressive strengths of around 17 MPa can be achieved within 7 days. The early age strengths of these samples were primarily attributed to the formation of hydrocalumite. With increasing curing duration, geopolymer gel, C-A-S-H, ettringite, and phillipsite were formed. Both C-A-S-H and phillipsite showed binding of chlorides. Only phillipsite showed sequestration of sulfates in the matrix. The calcined clay blends containing 50 to 75% kaolinite performed better than the samples containing 100% kaolinite in terms of reaction rate and compressive strengths.

1. Introduction

Ordinary Portland Cement (OPC)-based materials are often heavily criticized because of their high carbon footprint, energy-intensive manufacturing process, and consumption of freshwater (Monteiro et al., 2017; Scrivener et al., 2018; Miller et al., 2018). Most of these environmental impacts could be minimized using the construction materials used by ancient Roman engineers nearly 2000 years ago (addressed as 'Roman concrete' hereafter). Roman concrete offers a lower carbon footprint and lower freshwater consumption compared to OPC (Jackson et al., 2012a; Palomo et al., 2019; Yi et al., 2020). In addition to the environmental considerations, Roman concrete also represents the epitome of extremely durable cement-based materials, especially against seawater and alkali-silica reaction (ASR). Roman concrete exposed to harsh maritime environments remains in a remarkable condition even 2000 years after construction, while modern ordinary Portland cement (OPC) concrete shows degradation within 32 weeks of exposure to seawater (Santhanam et al., 2006; Yi et al., 2020). Finally, by replicating the role of reactive aggregates in Roman concrete, it may be possible to minimize the ASR (Rajabipour et al., 2015) damage of concrete. Accordingly, mimicking the hardening mechanisms and properties of Roman concrete using the currently available material sources presents a promising path towards the development of a durable, resilient, and sustainable marine concrete.

Several previous studies (Jackson et al., 2012; Jackson et al., 2013, 2014, 2017, 2018; Macfarlane et al., 2021) have provided comprehensive insights on the mineral formations and chemo-mechanical characteristics of Roman concrete. Based on these studies (Jackson et al., 2012b; Jackson et al., 2013, 2014, 2017, 2018), as well as recent trials to produce Roman concrete (Oleson et al., 2006; Gotti et al., 2008; Palomo et al., 2019) and other related studies (Pollio, 1914; Vanorio and Kanitpanyacharoen, 2015; Rhodes, 2018; Maragh et al., 2019), it is

* Corresponding author.
E-mail address: warda.ashraf@uta.edu (W. Ashraf).

https://doi.org/10.1016/j.clay.2022.106696
Received 18 February 2022; Received in revised form 28 August 2022; Accepted 30 August 2022
Available online 8 September 2022

known that Roman concrete was produced using a mixture of natural volcanic ash, slaked lime, and volcanic aggregates. It has been suggested that, in the presence of seawater, these ingredients went through a series of pozzolanic and post-pozzolanic reactions to form C-A-S-H, Al-tobermorite, and zeolitic phases in the matrix as well as in aggregate pores and interfaces (Jackson et al., 2017). While the binding phases present in Roman concrete are significantly different than those in OPC concrete (e.g., C-S-H and $Ca(OH)_2$), reaction products similar to those in Roman concrete can be obtained in alkali-activated materials (Provis and Bernal, 2014). Attempts to reproduce Roman concrete via alkali activation of aluminosilicates or lime-pozzolan binder reactions are not new (Vejmelková et al., 2012). A recent article (Palomo et al., 2019) summarized such attempts with the current level of understanding of Roman concrete. It is important to note that Roman concrete was essentially formed by mixing pozzolanic material (e.g., volcanic ash, aggregates) and portlandite (slaked lime) whereas modern efforts of replicating this ancient material have mostly involved using additional alkali activators, such as NaOH, Na_2SO_4, and Na_2SiO_3 (Palomo et al., 2019). This modification is understandable considering the lime-pozzolan binder often shows very slow reactivity and low strength (Hewlett and Liska, 2019). Due to the presence of alkali activators, the modern replicates often contain additional sodium-rich gel phases which are unlikely or present in lesser amounts in Roman concrete (Alonso and Palomo, 2001a; Alonso and Palomo, 2001b; Granizo et al., 2002; Garcia-Lodeiro et al., 2013; Palomo et al., 2019). The challenging aspect is that the commonly used alkali activators have high carbon footprints, and depending on the activator sources, some of these alternative cementitious materials may even pose a higher carbon footprint than OPC (Habert and Ouellet-plamondon, 2016). In addition to the activator use, the selection of appropriate pozzolanic material poses a challenge for the reproduction of Roman concrete. Past attempts at reproducing Roman concrete primarily used coal fly ash and blast furnace slag (Palomo et al., 2019). However, the availabilities of these raw materials, especially coal fly ash, are limited (or declining) in several regions in the world (Juenger et al., 2019).

Considering the above factors, in this work, calcined clay was used to mimic the cementation process of Roman concrete. Due to the abundant presence of natural clay deposits throughout the world, calcined clay is a more readily available pozzolanic material as compared to industrial by-products (Scrivener et al., 2018a; Maier et al., 2021). The applications of calcined kaolinite (i.e., metakaolin, MK) as a pozzolanic material or precursor of alkali-activated material have been heavily explored during the past few decades (Tironi et al., 2012; Juenger and Siddique, 2015; Khalifa et al., 2020). Multiple studies have shown that due to the high reactivity along with a high specific surface area, calcined kaolin can be used as an effective precursor (Yunsheng et al., 2010; Du and Pang, 2020; Ababneh et al., 2022). However, natural clay deposits contain various minerals in addition to kaolinite (Kaol) (Weems, 2022). Therefore, in this work, to ensure wider applicability of the raw material, calcined clay containing blended Kaol and montmorillonite (Mt) was used as the source of pozzolanic material. Furthermore, similar to Roman concrete, seawater was used for mixing and curing the calcined clay and portlandite paste batches without the presence of any other alkaline activators. Finally, the strength, micro and nano structural characteristics of the produced paste samples were evaluated and compared with those of Roman concrete. Briefly, the goals of this study were as follows: (i) evaluate the effectiveness of calcined clay containing blended minerals as the pozzolanic material to mimic the microstructure and mechanical performance of Roman concrete, and (ii) by mimicking the microstructure of the Roman concrete, provide a better understanding of the reactions that occurred in this ancient construction material in the early stage (up to 56 days).

2. Materials and methods

2.1. Raw materials

Kaol and Mt were procured from VWR. X-ray Diffraction (XRD) patterns of the powdered samples were obtained using a Cu Kα source. The diffraction patterns were obtained for the 2θ range from 5° to 60° using a step size of 0.02 (2θ) per second. Based on the XRD patterns (Fig. 1(a)), full amorphization of Mt was achieved after calcining at 900 °C for two hours. Partial amorphization of this clay mineral was achieved after 750 °C. In the case of Kaol, full amorphization was achieved after calcining at 750 °C for two hours (Fig. 1(b)). Accordingly, the clay blends were calcined at 750 °C to achieve full reactivity of Kaol, partial reactivity of Mt, and to avoid recrystallization of Kaol. The calcined clay was then used as the pozzolanic material to recreate the cementing process of Roman concrete. The XRD patterns of raw clay minerals also confirmed the absence of any impurity (e.g., quartz) in these materials (Fig. 1 a,b). The particle size distributions of the calcined clays, as obtained using a laser particle size analyzer, are shown in Fig. 1 (c). The d_{50} were 20.16 μm and 36.16 μm for calcined kaolin and calcined montmorillonite respectively. Calcined kaolin particles were 1.8 times finer than the montmorillonite. The oxide contents of the clay samples are shown in Table 1.

2.2. Mix batches

A series of mix batches with variable (i) pozzolan (i.e., calcined clay) to portlandite ratios (2:1 to 4:1) and (ii) clay mineral ratios (Kaol and Mt) were prepared. Details of these mixture series are given in Table 2. The calcined clay to portlandite ratios were selected based on ancient texts on Roman concrete (Pollio, 1914). Artificial seawater, prepared as per ASTM D1141 (Table 3), was then added to the dry mixtures of calcined clay and portlandite to achieve paste like consistency. Several trial batches were prepared to identify the optimum seawater to binder ratio as shown in Fig. 2. The optimum seawater to binder (portlandite + calcined clay) ratio to achieve such consistency was found to be 0.60. The samples were cured in seawater at room temperature. The samples were taken out of the seawater at specific durations (7 days, 28 days, 56 days). The hydration reaction of the samples was arrested by the solvent exchange method and isopropanol was used in this procedure.

2.3. Experimental methods

2.3.1. Thermogravimetric analysis (TGA)

The commercially available TGA 550 TA instrument was used in this study. Paste samples were first ground using a mortar and pestle, and then approximately 35– 40 mg of ground powder sample was loaded into a platinum pan and kept in an isothermal condition at around 25 °C for 5 min. Afterwards, the temperature of the TGA chamber was increased to 980 °C with a ramp of 15 °C per minute. N_2 gas was purged in the entire process. Initially, for a few batches, three replicate samples were tested through TGA to validate for any deviation in carbonation across samples. The test result deviations were less than 2% by weight of the samples. Due to the low deviation, TGA was performed with only one sample for the remainder of the batches. The following decomposition temperatures were used for analysis of the TGA data in this current study: chemically bound water decomposes between 100 and 600 °C (Villain et al., 2007; Deboucha et al., 2017; Scrivener et al., 2018b), chemically bound water usually implies the water which combines with different phases of binder, and $Ca(OH)_2$ decomposes to CaO and H_2O at around 450 °C (Villain et al., 2007; Scrivener et al., 2018b).

2.3.2. Isothermal calorimeter

First, dry mixtures of portlandite and calcined clay were prepared as per the proportions given in Table 2. Approximately 15 g of the dry mix sample was put in a glass vial and then placed inside an isothermal

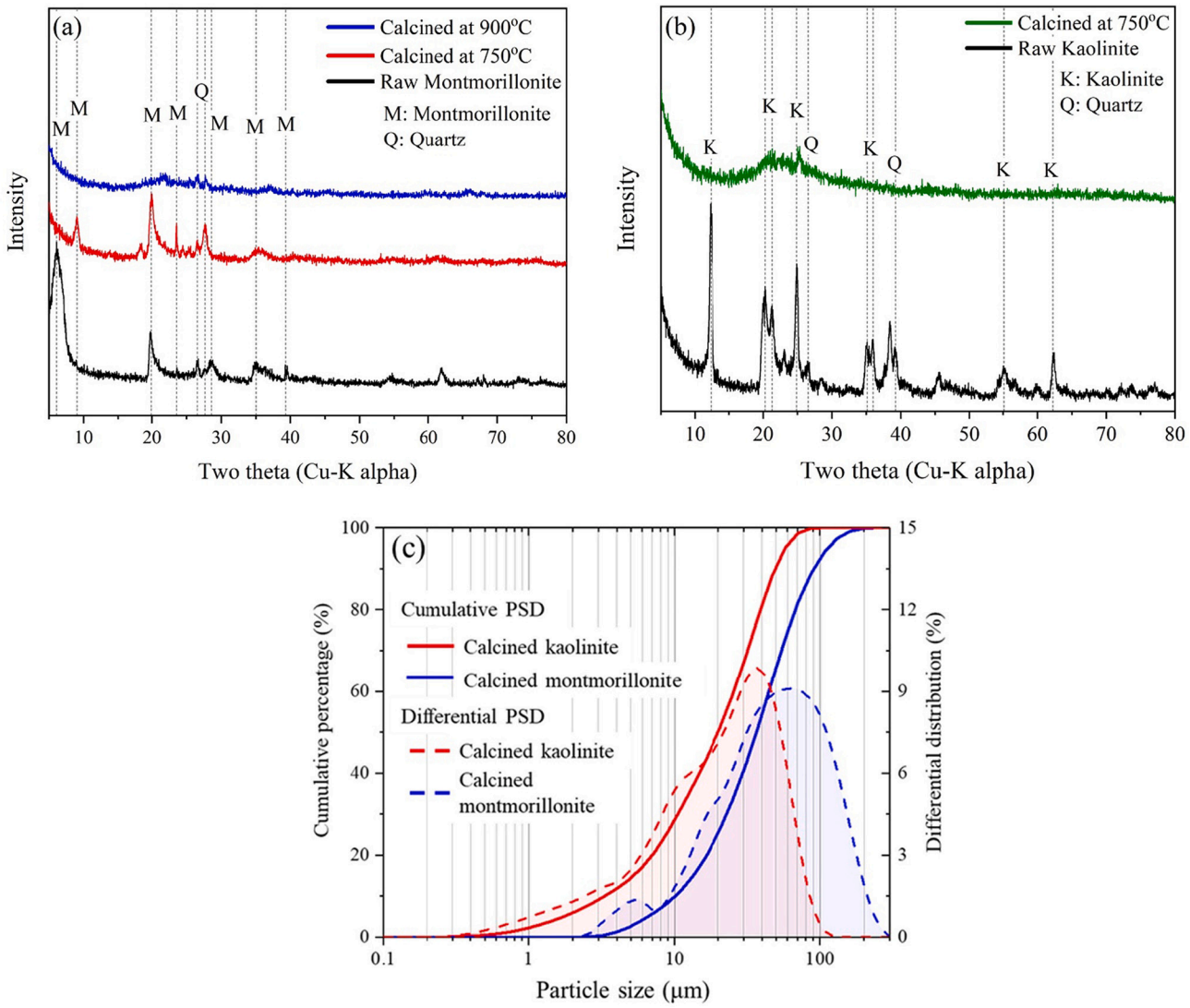

Fig. 1. Raw material characterization: (a) XRD pattern of Mt, (b) XRD pattern of Kaol, and (c) particle size.

Table 1
Oxide contents (weight %) of the clays.

	SiO_2	Al_2O_3	Fe_2O_3	CaO	MgO	Na_2O	K_2O
Kaolinite	53.06	42.9	0.92	0.06	0.14	0.04	0.29
Montmorillonite	64.37	22.47	4.24	1.71	2.35	0.60	0.22

Table 2
Mixture IDs and compositions.

Mix ID	Calcined kaolinite to montmorillonite ratio	Calcined clay to portlandite ratio
M1	100:0	2:1
M2	50:50	2:1
M3	75:25	2:1
M4	100:0	3:1
M5	50:50	3:1
M6	75:25	3:1
M7	100:0	4:1
M8	50:50	4:1
M9	75:25	4:1

Table 3
Composition of artificial seawater as per ASTM D1141.

Compound	Concentration, g/L	Compound	Concentration, g/L
NaCl	24.53	$Ba(NO_3)_2$	0.0000994
$MgCl_2$	5.20	$Mn(NO_2)_2$	0.0000340
Na_2SO_4	4.09	$Cu(NO_3)_2$	0.0000308
$CaCl_2$	1.16	$Zn(NO_3)_2$	0.0000096
KCl	0.695	$Pb(NO_3)_2$	0.0000066
$NaHCO_3$	0.201	$AgNO_3$	0.00000049
KBr	0.101		
H_3BO_3	0.027		
$SrCl_2$	0.025		
NaF	0.003		

calorimeter (TAM Air, TA instrument) to monitor the heat of hydration. After placing the samples inside the calorimeter, it needed around 45 min to stabilize the heat flow signals. Once the signals were stabilized, seawater (or deionized water) was injected to the dry mix using syringes. In this approach, the heat of reaction was obtained starting immediately after adding the water and continuing up to about 7 days. The heat of reaction measurements was collected at an ambient temperature of 23 °C.

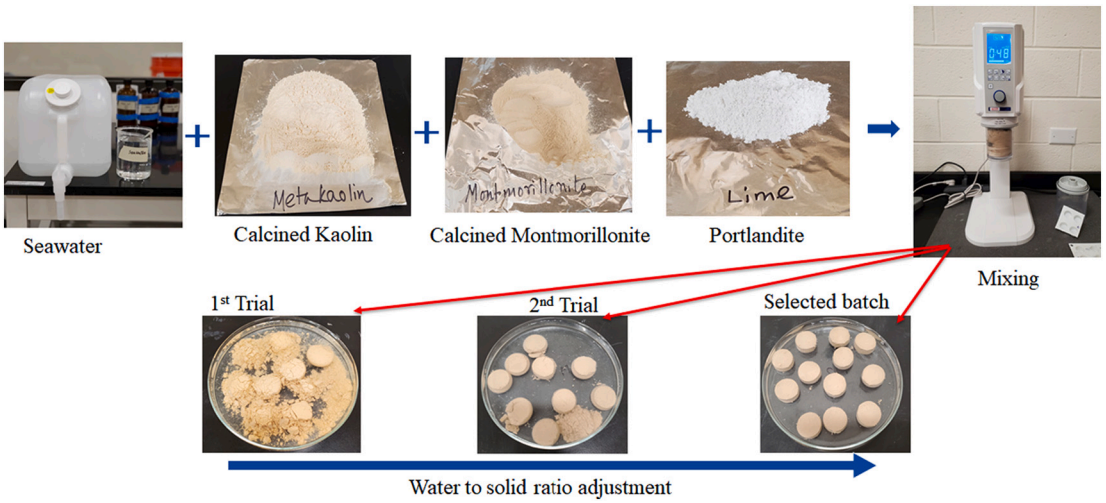

Fig. 2. Pictures showing the sample preparation steps and the identification of optimum seawater to binder ratio.

2.3.3. Scanning electron microscope - energy dispersive spectroscopy (SEM-EDS)

The microstructure of the calcined clay-portlandite pastes was evaluated using the Hitachi 3000 N SEM. The instrument was operated in high-vacuum mode with a 30-kV accelerated voltage and a working distance of about 10 mm. The cement paste sample was coated with Platinum (Pt) before capturing the SEM images. This experiment was carried out on the fractured surface of the paste samples.

2.3.4. Solid state nuclear magnetic resonance (NMR)

All the ^{27}Al solid-state NMR experiments were conducted at 17.6 T on a Varian VNMRS 750 MHz spectrometer at the SCS NMR Facility of the University of Illinois at Urbana-Champaign, operating at resonance frequency of $\nu 0$ (^{27}Al) = 195.4 MHz, at room temperature. A Varian 4 mm triple-resonance HXY T3 Narrow Bore (NB) magic-angle spinning (MAS) probe was used for all MAS experiments under spinning rates of 7–15 kHz. All samples were finely ground and packed into 4 mm o.d. standard zirconia rotors (typically around 60–85 mg). Experimental aluminum chemical shift referencing, pulse calibration and setup were done using 1 M $Al(NO_3)_3$ solution, which has a chemical shift of 0.00 ppm. The ^{27}Al pulse width used was 1.67 μs, which is the selective 90-degree pulse for $I = 5/2$ (based on the non-selective 90 degree of 5 μs). A recycle delay of 1 s or 5 s was used and 256–1400 scans were acquired for each sample.

All the ^{29}Si solid-state NMR experiments were conducted at 7.05 T on a Varian Unity Inova 300 MHz spectrometer at the SCS NMR Facility of the University of Illinois at Urbana-Champaign, operating at resonance frequency of $\nu 0$ (^{29}Si) = 59.6 MHz, at room temperature. A Varian/Chemagnetics 7.5 mm double-resonance APEX HX magic-angle spinning (MAS) probe was used for all MAS experiments under spinning rate of 4 kHz and TPPM 1H decoupling. All samples were finely ground and packed into 4 mm o.d. standard zirconia rotors (typically around 210–580 mg). Experimental silicon chemical shift referencing, pulse calibration and setup were done using powdered octakis(trimethylsiloxy)silsesquioxane (Q8M8), which has a chemical shift of 11.45 ppm, relative to the primary standard, TMS at 0 ppm. The ^{29}Si pulse width used was 1.5 μs, corresponding to a 45-degree pulse. A recycle delay of 30s was used and 1920 scans were acquired for each sample. The equation for calculation of Si/Al ratio and degree of reaction (δ_{si} and δ_{Al}) can be found in previous studies (Gao et al., 2017; Lin et al., 2021).

2.3.5. X-ray diffractions

X-ray Diffraction (XRD) patterns of the powdered samples were obtained using a Cu Kα source. The diffraction patterns were obtained for the 2θ range from 5° to 60° using a step size of 0.02 (2θ) per second.

2.3.6. Compressive strengths

The compressive strengths of the 25 mm cube samples prepared from the paste were measured after 7, 28, 56, and 90 days of submerged curing in seawater at room temperature. The compressive strength was measured via the MTS Landmark servo hydraulic test system using a displacement rate of 0.02 mm/s.

3. Results

3.1. Heat of reaction

Fig. 3 shows the heat of reaction values of the calcined clay-portlandite mixture with the addition of seawater. Worthy to note, similar measurements were performed in the case of deionized water addition in calcined clay and portlandite mixtures (supplementary Fig. S.1). However, it was evident that the heat of reaction for such a system was significantly increased due to the use of seawater instead of deionized water. Such acceleration effect due to the addition of seawater can be attributed to the presence of chloride and sulphate ions in the system. Accordingly, it can be postulated that the seawater acts as an activator for such a portlandite - calcined clay binder system. The seawater-containing batches also showed two distinct peaks in the heat flow measurements (Fig. 3b). The first intense heat flow peak, immediately after the addition of seawater, can be attributed to the dissolution of the solid phases (i.e., calcined clay and portlandite). The second heat flow peak appeared from 2 to 50 h after the addition of seawater. This second heat flow peak appeared to be similar to those typically observed in the case of OPC hydration reactions. Among the seawater-containing batches (Fig. 3a), the highest heat release was obtained from the M3 batch, which contained a 75:25 proportion of calcined Kaol and Mt along with a calcined clay to portlandite ratio of 2:1. On the other hand, the highest heat flow peak was obtained from the M4 batch that contained calcined Kaol and portlandite in a 3:1 ratio (no Mt). Therefore, the rate of reaction in such systems depends on the relative combinations of calcined clay minerals and portlandite, and a direct correlation with only one ingredient can be misleading. Regardless, it was observed that the heat release from the batches containing a calcined clay-to-portlandite ratio of 4:1 was very low, indicating there was not enough portlandite in these systems to continue the reaction.

3.2. Portlandite consumptions

To understand the consumption rate of portlandite in the produced system, thermogravimetric analyses (TGA) were performed. A typical TGA plot with the decomposition temperatures of various hydrous

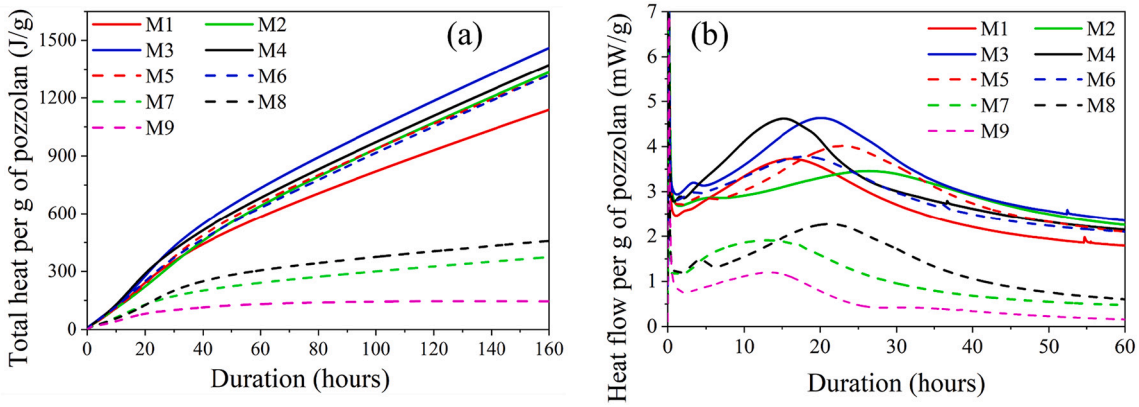

Fig. 3. Heat of reaction of calcined clay-portlandite mixtures after the addition of seawater.

phases is shown in Fig. 4 (a). The decomposition temperatures for the cement hydration products were selected based on previously published data (Scrivener et al., 2018b). The amounts of portlandite present in the paste samples were calculated from derivative thermogravimetric (DTG) plots using a method published elsewhere (Scrivener et al., 2018b). It is important to note that portlandite decomposes at about 400 to 500 °C and brucite decomposes around 360 °C. Nevertheless, based on the DTG/TGA measurements, the overall weight loss in the temperature range of 350 to 500 °C was low, and any attempt to separate brucite and portlandite was avoided. It can be observed from Fig. 4 b, the starting solid mixtures (pozzolan + portlandite) contained around 20 to 33% of the portlandite. However, only the M1, M2, and M3 batches were found to contain unreacted portlandite after 3 days. Among these batches, full consumption of portlandite was achieved within 28 days for the M1 and M3 batches, which contained relatively higher calcined Kaol content compared to the M2 batch (Table 2). The M2 batch was found to have around 2% unreacted portlandite even after 56 days of curing in seawater. Considering the M2 was prepared using a 1:1 ratio of calcined Kaol (high reactivity) and Mt (low reactivity), this low consumption rate of portlandite was expected. All other sample batches (M4 to M9) showed complete consumption of portlandite after 3 days of curing. This finding confirms that in the presence of seawater, the reaction between portlandite and calcined clay occurs rather rapidly.

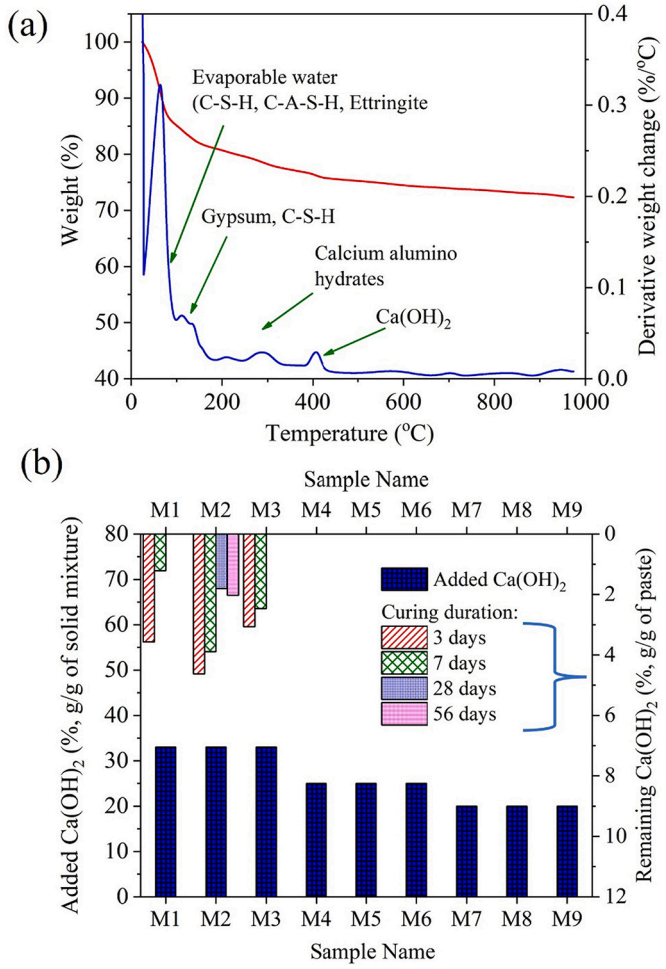

Fig. 4. (a) Typical TGA plots for a calcined clay-portlandite mixture cured in seawater and (b) relative amounts of portlandite present in the mixtures before and after seawater curing.

3.3. Mineralogy of crystalline reaction products

3.3.1. Effects of blended clay minerals

Fig. 5 shows the crystalline microstructural phase evolution in the calcined clay-portlandite paste samples for different clay-mineral blending ratios. It is important to note that all of these systems had more than 80% by weight amorphous phase. The nature and arrangements of these amorphous phases are discussed in Section 3.4. Other than the amorphous phases, a variety of crystalline products were identified in these systems. Identification of these phases were also compared with those reported in previous studies for similar binder systems (Hewlett and Liska, 2019). As observed from Fig. 5 a, within 3 days of preparation and curing, the calcined Kaol-portlandite paste formed a significant amount of hydrocalumite [$[Ca_2Al(OH)_6]Cl{\cdot}2H_2O$, Friedel's salt], a layered double hydroxide (Leroux et al., 2002; Gevers and Labuschagné, 2020). This mineral phase was formed by the reaction of alumina from calcined clay, calcium from portlandite, and chloride from seawater. Formation of hydrocalumite has also been reported to form in Portland cement concrete in the presence of seawater and metakaolin (Li et al., 2015). Additionally, a C-S-H (or C-A-S-H) type phase was also identified by the broad peak at around 29° two-theta. Other calcium- and alumina-bearing mineral phases, including grossular [$Ca_3Al_2(SiO_4)_3$] and grossite [$(CaAl_4O_7)$] were formed after 3 days of curing. Only a small amount of gypsum was found to be present in this system. Interestingly, phillipsite was found to occur in the 3 days cured samples. It is important to note that phillipsite is a zeolite mineral that was also found in ancient Roman concrete (Jackson et al., 2017). Finally, okenite [$CaSi_2O_5{\cdot}2H_2O$], a hydrated calcium silicate mineral associated with zeolite was also found in this system. Okenite is not traditionally found in portland cement based systems, but previous studies have shown formation of this phase in 30-year old concrete (Cole and Lancucki, 1983). After 7 days of curing, the paste samples contained similar

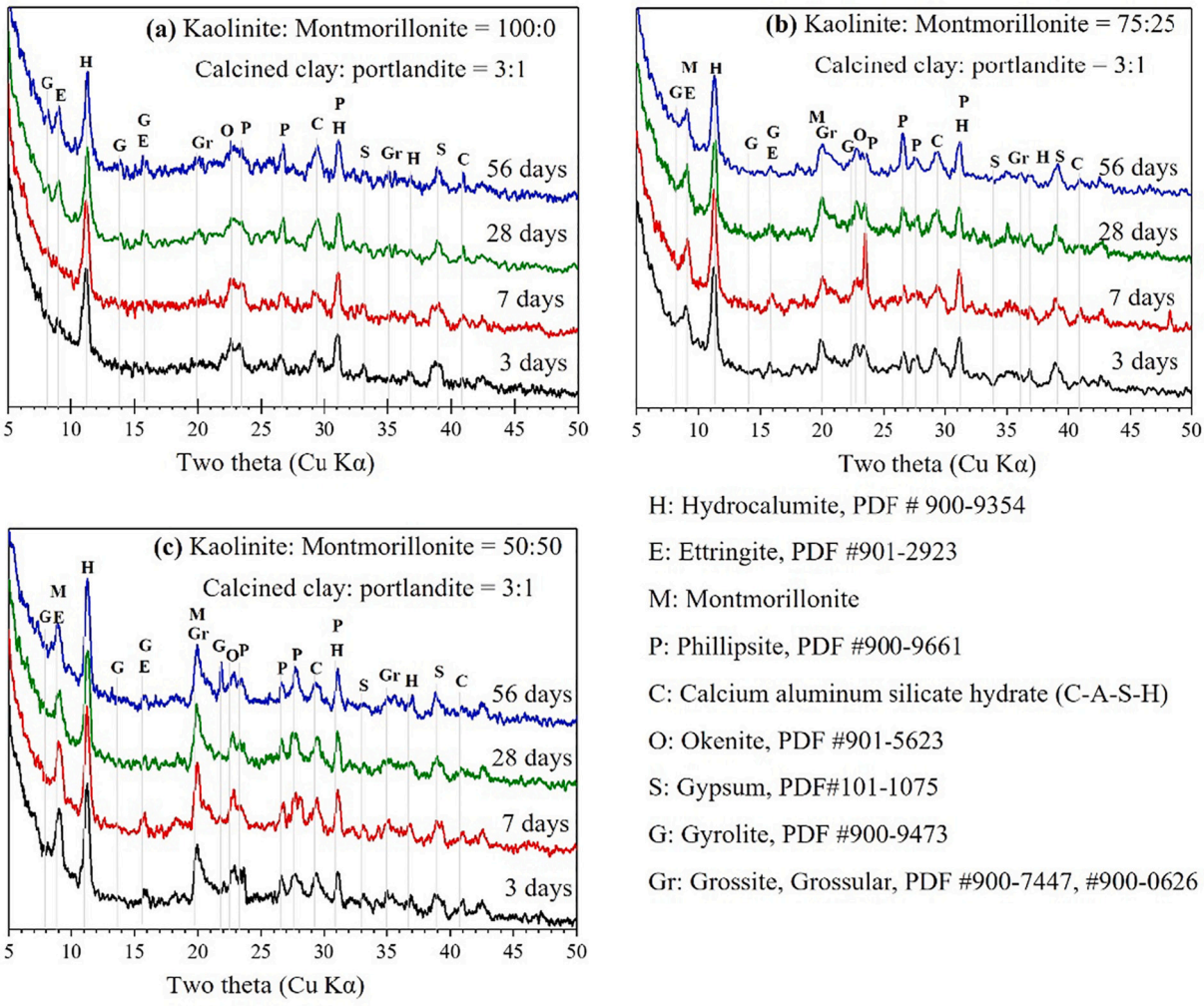

Fig. 5. XRD patterns of seawater-cured calcined clay-portlandite paste samples, (a) Kaol to Mt ratio of 100:0 – mix M4, (a) Kaol to Mt ratio of 75:25 – mix M6, and (c) Kaol to Mt ratio of 50:50 – mix M5. Calcined clay to portlandite ratio for all these mixes was 3:1.

mineral phases as listed above, but with a slightly higher intensity. Two new mineral phases were formed after 28 days of curing, including ettringite [$Ca_6Al_2(SO_4)_3(OH)_{12}{\cdot}26H_2O$] and gyrolite [$NaCa_{16}O_{60}(OH)_8{\cdot}14H_2O$]. Formation of ettringite was associated with a decrease in the intensity of gypsum. Ettringite is known to be an expansive mineral and often causes cracking of the matrix due to such expansion. However, within the tested duration, the presence of ettringite did not show any detrimental effect on the strength. The presence of gyrolite had previously also been reported in alkali activated dicalcium silicate systems (Ashraf, 2018). After 56 days of curing, the intensities for gyrolite, ettringite, hydrocalumite, okenite, and phillipsite were increased without causing any other major mineral phase formation. Interestingly, stratlingite ($Ca_2Al_2SiO_7.8H_2O$), a commonly found mineral in lime-pozzolan binder systems (Frías et al., 2020), was not found in the produced paste samples. It should be noted that multiple factors such as amounts of portlandite, age of specimen, and purity of clay affect the formation of stratlingite. The combination of all the aforementioned factors can be the cause of the absence of stratlingite in the present study (Krishnan et al., 2019; Dhandapani and Santhanam, 2020; Alberto and Sommariva, 2020; Shah et al., 2022).

The mineral phases present in the paste samples containing blended clay minerals (Fig. 5b and Fig. 5c) were similar to those observed in the case of the pure calcined Kaol batch (Fig. 5a). However, with an increase in the calcined Mt content, the intensities of hydrocalumite and phillipsite increased as well. It is important to note that Kaol has a higher alumina content (Si:Al = 1:1) compared to the Mt (Si:Al = 2:1). Therefore, formation of higher amounts of the alumina-bearing phase with increased amount of Mt was counterintuitive. We suggest that due to slow reactivity of calcined Mt, addition of this mineral to calcined Kaol caused a dilution. As such, the concentration of chlorides and seawater ions per unit weight of calcined Kaol were higher in the case of the Mt containing batches. Because of this dilution effect, higher amounts of the alumina-bearing phases were formed in the case of the blended clay minerals batches.

3.3.2. Effects of the calcined clay to portlandite ratios

The effects of the calcined clay-to-portlandite ratios on the mineralogy are presented in Fig. 6. With increasing proportions of calcined clays, the amount of hydrocalumite was increased in the paste after 3 days of curing. However, in the case of the 2:1 calcined clay-to-portlandite ratio (Fig. 6a), the amounts of hydrocalumite kept increasing within the tested duration. On the other hand, in the case of higher pozzolan contents (Fig. 6b and Fig. 6c), the amount of hydrocalumite increased until 7 days, after which it started decreasing. Based on the XRD patterns, after 7 days of curing, the supply of calcium ions (from portlandite) was depleted which caused the dissolution of hydrocalumite and formation of ettringite. Accordingly, after 56 days of curing, the paste batch with the lowest portlandite ratio resulted in the formation of the highest amount of ettringite and the lowest amount of hydrocalumite. The relative intensities of phillipsite were also observed

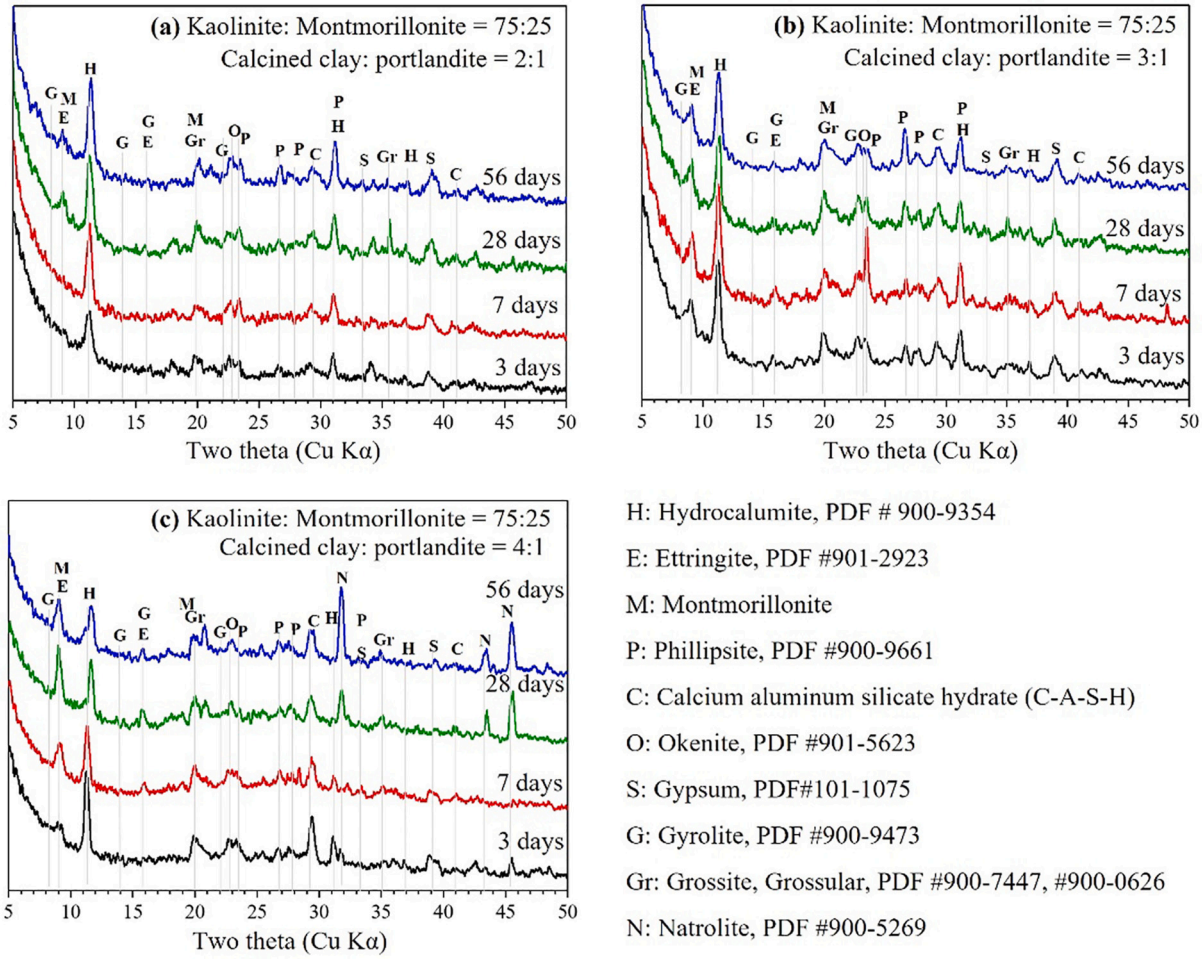

Fig. 6. XRD patterns of seawater-cured calcined clay-portlandite paste samples, (a) calcined clay to portlandite ratio of 2:1 – mix M3, (a) calcined clay to portlandite ratio of 3:1 – mix M6, and (c) calcined clay to portlandite ratio of 4:1 – mix M9. Calcined Kaol to Mt ratio for all these mixes was 75:25.

to decrease with decreasing amounts of portlandite in the mixture. Interestingly, at the lowest portlandite content (calcined clay: portlandite = 4:1, Fig. 6c) the paste matrix was found to contain halite (NaCl) after 28 days of curing. The presence of halite indicates that Na^+ and Cl^- ions are retained in the diffused layer of reaction products. The relative amounts of C-S-H were also decreased with decreasing amounts of portlandite content in the mixture. Since the relative amounts of C-S-H was lower, this allowed the easier formation of halite in the lowest portlandite mix.

3.4. Characterization of amorphous reaction products

3.4.1. Observations from ^{29}Si MAS NMR

The ^{29}Si and ^{27}Al solid-state nuclear magnetic resonance (NMR) spectra of calcined Kaol and Mt are presented in Fig. 7. As expected from previous studies (Slaty et al., 2013; Garg and Skibsted, 2019; Khalifa et al., 2020), calcined Kaol and calcined Mt were primarily found to contain highly polymerized $Q^4(n\text{Al})$ structural units (where, n = 0,1,2,3,4 etc.). Fig. 8 shows the ^{29}Si NMR spectra of the M4, M5, and M6 paste batches after 56 days of curing in seawater. All of these samples were found to contain overlapping peaks in the range of – 80 ppm to −120 ppm. The relatively high intensity of the Q^1 peak, in addition to the Q^3 and Q^4 peaks, indicate the co-existence of C-A-S-H and geopolymer gel. The coexistence of C-A-S-H and geopolymer gel in portlandite and metakaolin mixtures has also been reported in the past (Chen et al., 2018). In the presence of soluble Ca, it is expected that C-A-S-H and geopolymer gel will co-exist in the alkali-activated material (Yip et al., 2005, 2008; Puligilla and Mondal, 2015). Considering the co-existence of C-A-S-H and geopolymer gel, the ^{29}Si NMR spectra of the paste samples were then deconvoluted and the assigned peaks are listed in Table 4. The nomenclature of peak as well as the equations for the calculation of the Si/Al ratio and reaction degree can be found in previously published studies (Kobera et al., 2014; Chen et al., 2018; Walkley and Provis, 2019; Zhang et al., 2020; Lin et al., 2021).

The Si/Al values given in Table 4 represent the average Si atoms connected to tetrahedral Al atoms. It can be observed that the incorporation of calcined Mt results in higher Si/Al values compared to the 100% calcined Kaol clay batch. In general, the aluminosilicate gel is divided into two categories: Gel 1 is Al-rich and Gel 2 is Si-rich (Duxson et al., 2007). It is suggested that Gel 1 forms in the first stage of the alkaline activation and eventually converts to Gel 2 with Si-enrichment with the increased degree of reaction. Additionally, the formation of Gel 2 is expected to result in better mechanical performance (Duxson et al., 2007), as was also observed in the compressive strength measurements of the calcined clay-portlandite batches (details in Section 3.6).

As seen in Table 4, the reaction degree (δ_{si}) was highest for the calcined clay blend containing Kaol: Mt of 75:25 followed by 50:50 and then 100:0 blends. Therefore, for such calcined clay-portlandite systems, the presence of Mt offers a higher degree of reaction than the pure Kaol batch. However, it should be noted that a higher amount of montmorillonite clay slightly lowers the reaction degree. This can be due to the dilution effect caused by the reduced amount of Kaol. Nevertheless, the reaction degree of all geopolymer mixes containing Mt clay was higher than of the 100% Kaol clay batches. Furthermore, the presence of

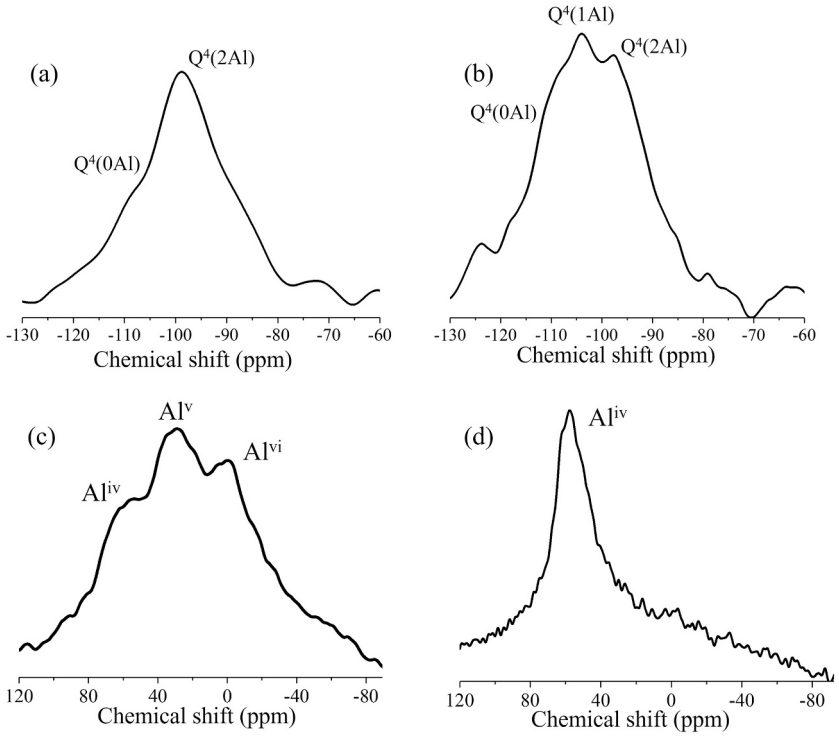

Fig. 7. (a) ^{29}Si NMR spectra of calcined Kaol, (b) ^{29}Si NMR spectra of calcined Mt, (c) ^{27}Al MAS NMR spectra of calcined Kaol, and (b) ^{27}Al MAS NMR spectra of calcined Mt.

hydrocalumite and phillipsite in XRD patterns also indicated that addition of Mt leads to a slightly higher degree of reaction.

3.4.2. *Observations from ^{27}Al MAS NMR*

The ^{27}Al NMR spectra of calcined Kaol and calcined Mt are shown in Fig. 7 (c and d). The three peaks are usually indicative of Al^{vi} (6-coordinated), Al^{v} (5-coordinated), and Al^{iv} (4-coordinated) structures of the aluminosilicates present in the calcined clays. These characteristic arrangements of Al in calcined Kaol and calcined Mt match previously reported observations (Fernandez et al., 2011).

Fig. 9 shows the ^{27}Al NMR spectra of calcined clay and portlandite paste samples cured in seawater for 56 days. The peaks in the chemical shift ranges of 9 to 15 ppm, 20 to 40 ppm, and 60 to 80 ppm were attributed to the presence of Al^{vi}, Al^{v}, and Al^{iv} arrangements in the hydrated samples. The broad peaks observed in calcined Kaol and calcined Mt (Fig. 7) were shifted to different positions after the alkali activation using seawater and portlandite. The sharp new peak at 9 ppm was assigned to hydrocalumite and other calcium aluminate hydrate phases formed in this system, as also identified using XRD. The peak at 13 ppm was assigned to the Al arrangement in ettringite based on the literature (Skibsted et al., 1993; Faucon et al., 1998). The narrow width of these two peaks also indicates a well-ordered octahedral structure confirming the presence of Al-bearing crystalline reaction products. The broad peak around 64 ppm represents the tetrahedral coordination of Al in C-A-S-H and geopolymer gel (Wang and Scrivener, 2003; Sevelsted and Skibsted, 2015). The Al^{v} sites observed around 33 ppm were also assigned to C-A-S-H and geopolymer gel. Based on the ^{27}Al NMR spectra, there is not any significant difference in the paste samples prepared with different blending ratios of Kaol and Mt.

3.5. *Microstructural observations*

Fig. 10 shows the typically observed microstructural phases present in calcined clay-portlandite paste samples cured in seawater. With different curing durations and mix proportions, the relative amounts of the mineral phases varied; however, there was not any new phase formation. The most abundant products in these systems are the platy phases as shown in Fig. 10 (a to d), with a composition of calcium, aluminum, and silicates. This phase was identified as C-A-S-H with bound chloride contents. The C-A-S-H phase also appeared to sequester certain amounts of Na in it. It is worth noting that this phase should not be confused with stratlingite, which also has similar composition and plate morphology, considering that the XRD patterns did not show the presence of this phase. Ettringite needles were also identified in the calcined clay-portlandite paste samples. However, any excessive deposition of this phase or formation of expansive cracks were not observed. It is possible that the ettringite needles were intermixed with the C-A-S-H phase as indicated by the presence of Si in EDS. The geopolymer gel (N-A-S-H with a trace amount of calcium) was also observed in this calcined clay-portlandite system. The presence of this type of gel was confirmed by the NMR data (Fig. 7). The most interesting observation was the formation of calcium rich phillipsite. Phillipsite needles were abundant in this system, which primarily deposited in the pores. The morphology of the formed phillipsite was similar to those observed in ancient Roman concrete (Jackson et al., 2017). Phillipsite was also observed to sequester sulfates and chlorides, similar to that of Roman concrete.

3.6. *Compressive strengths*

Fig. 11 shows the compressive strengths of the calcined clay-portlandite paste samples cured in seawater. After 56 days of curing, the compressive strengths of the paste samples were in the range of 15 to 25 MPa. This strength is significantly higher than those achieved during past attempts to recreate Roman concrete using fly ash (Palomo et al., 2019), previous studies on calcined clay-lime binder activated with NaOH (Boonjaeng et al., 2014), and traditional lime-pozzolans binders (Massazza, 1993; Hernandez et al., 1998; Mccarthy and Dyer, 2019). The relatively higher strengths of the produced calcined clay-lime composites can be attributed to the fast reaction between Al present in

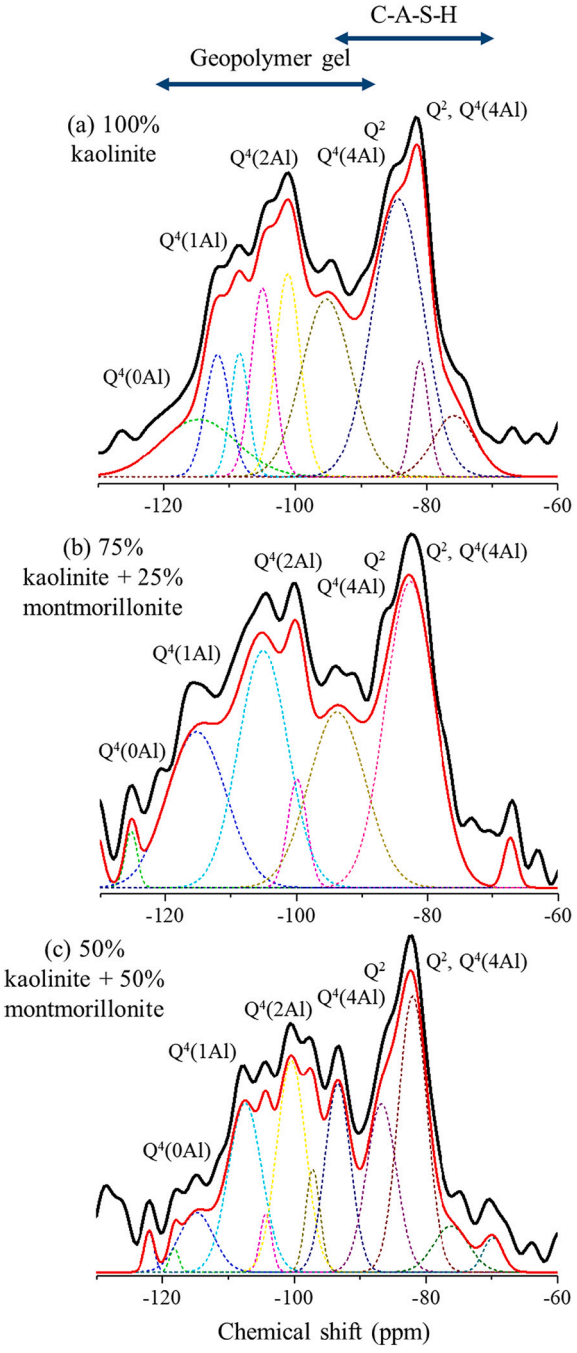

Fig. 8. ^{29}Si MAS NMR spectra of seawater-cured calcined clay-portlandite paste samples, (a) Kaol to Mt ratio of 100:0 – mix M4, (a) Kaol to Mt ratio of 75:25 – mix M6, and (c) Kaol to Mt ratio of 50:50 – mix M5. Calcined clay to portlandite ratio for all these mixes was 3:1.

clay and the minerals present in seawater. It is also important to note that this system achieved a moderate strength of around 17 MPa within only 7 days of curing in seawater. The relatively rapid hardening of this system compared to the typical lime-pozzolan binder is attributed to the presence of seawater, which led to the formation of hydrocalumite and phillipsite in this system. Based on this work, it is evident that in the case of lime-pozzolan binder mixed and cured with seawater, the first reaction that leads to the hardening is the mineralization of ions present in seawater. However, it is expected that such mineralization also depends on the relative amounts of alumina present in the system.

Interestingly, among the calcined clay-portlandite batches, the maximum compressive strength (~25 MPa) after 90 days of curing was

Table 4
^{29}Si NMR peak assignments and relative proportions of peak areas.

Phases	ppm	Peak assignment	Peak area proportions		
			Calcined kaolinite: Calcined montmorillonite ratios		
			100:0	50:50	75:25
			M4	M5	M6
C-A-S-H	– 80	Q1 (0Al)			
	– 82 to – 85	Q^2_p(0Al), Q^2_p(0Al), Q^2_p(1Al)			
Geopolymer gel	– 80 to – 85	Q^4 (4Al)	44.22	29.81	28.42
	– 85 to – 95	Q^4 (3Al)	8.49	11.34	15.01
	– 95 to – 100	Q^4 (2Al)	17.44	18.19	14.84
	– 100 to – 105	Q^4 (1Al)	7.57	8.84	20.60
	– 105 to – 120	Q^4 (0Al)	13.24	31.82	21.11
Si/Al ratio			1.63	1.91	2.01
δ_{si} (%)			11.05	16.18	18.02
δ_{Al} (%)			77.61	81.44	85.09

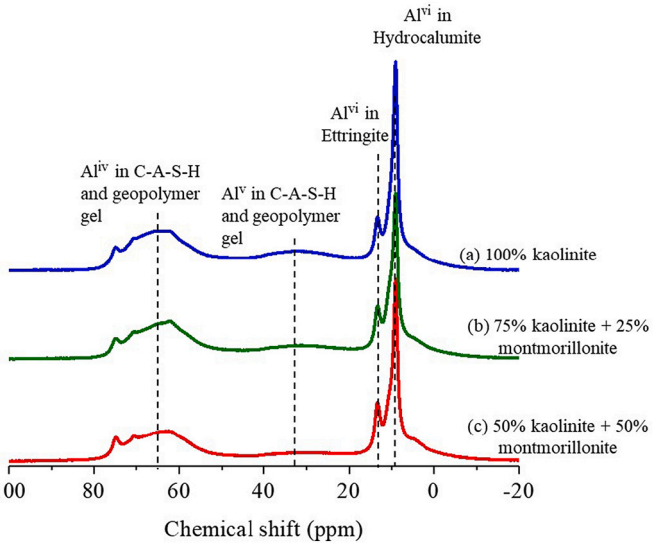

Fig. 9. ^{27}Al MAS NMR spectra of seawater-cured calcined clay-portlandite paste samples, (a) Kaol to Mt ratio of 100:0 – mix M4, (a) Kaol to Mt ratio of 75:25 – mix M6, and (c) Kaol to Mt ratio of 50:50 – mix M5. Calcined clay to portlandite ratio for all these mixes was 3:1.

obtained from the M3 mixture that contained the lowest calcined clay-to-portlandite ratio (2:1) and Kaol -to Mt blending ratio of 75:25. For different calcined clay-portlandite ratios, the highest 90-days compressive strengths were consistently obtained from 75:25 Kaol to Mt blending ratio. This observation matches the NMR finding that the paste batches with 75:25 Kaol to Mt ratio attained highest degree of reaction. Important to note, none of the batches showed decrease in the compressive strength after 90 days of curing, even though there was an increase in ettringite formation. Therefore, we suggest that all of the crystalline phases, including ettringite, phillipsite, and hydrocalumite, contributed positively to the strength after 90 days of curing.

4. Discussions

The findings of this study show that calcined clay is a viable option to produce seawater concrete by mimicking the cementation of Roman concrete. However, since the chemical composition of calcined clay is unlikely to be similar to the volcanic ashes that were used by the ancient

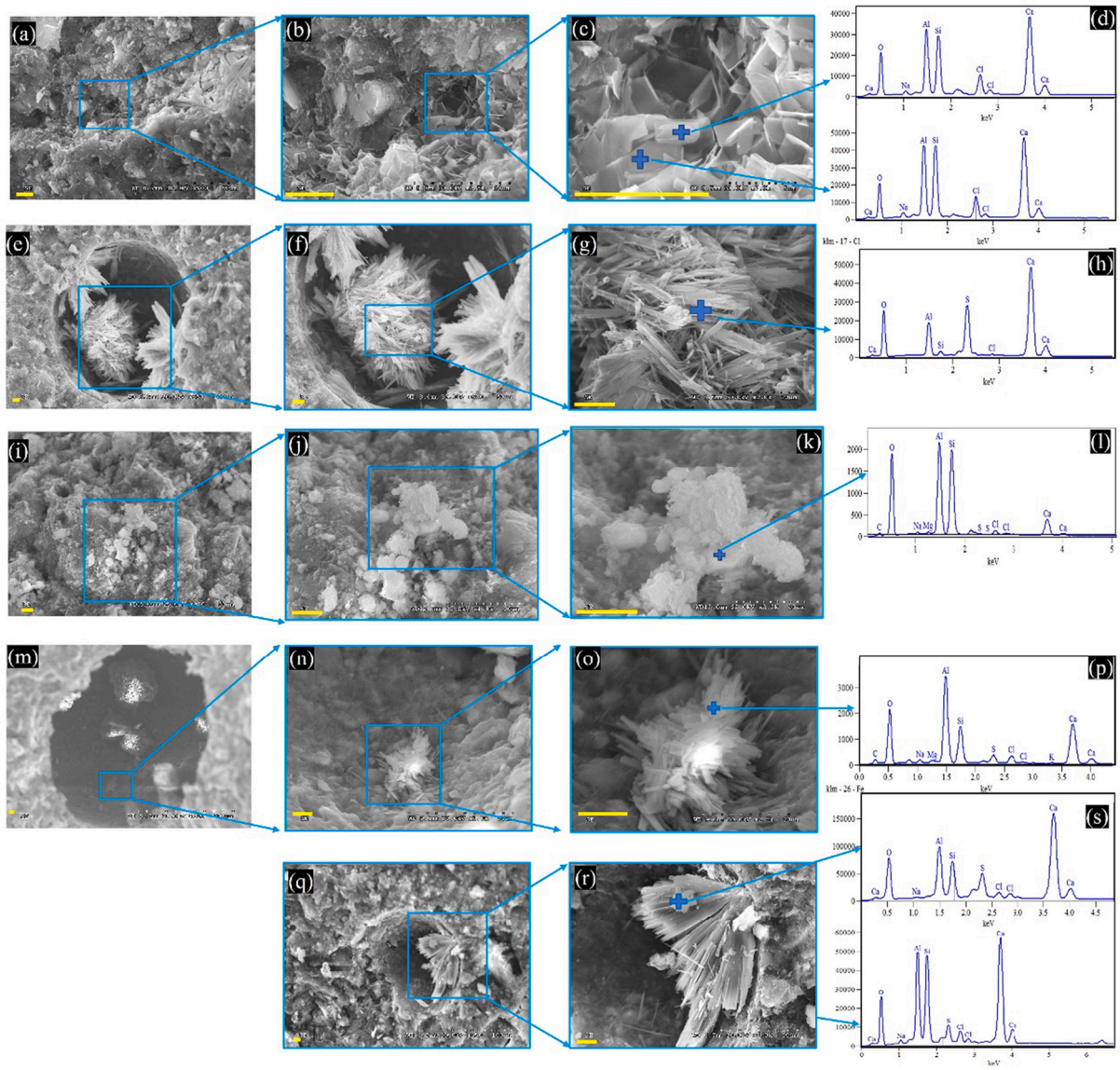

Fig. 10. SEM images with EDS showing different microscopic phases present in calcined clay-portlandite system: (a to d) platy C-A-S-H phase, (e to h) ettringite needles, (i to l) geopolymer gel, (m to s) phillipsite needles. The scale bar represents 10 microns

Roman engineers, it is understandable that the microstructure of the samples produced in this work is not exactly similar to that of Roman concrete. Comparing the ^{29}Si NMR spectra of the calcined clay-portlandite system (Fig. 8) with those of Roman concrete (published in (Jackson et al., 2012b), shown in supplementary Fig. S.2), it is apparent that the developed system contains more polymerized binding phase as evident by the broad peaks present in the range of – 90 to – 120 ppm. Therefore, although the presence of C-A-S-H (peaks around – 70 to – 90 ppm) are the same in both of these systems, the developed mixture contains additional geopolymer gel, which was not present in the Roman concrete. Additionally, based on the ^{27}Al NMR, the developed system contains crystalline ettringite and hydrocalumite with Al in octahedral coordination as evidenced by the peaks at 9 and 13 ppm (Fig. 9). On the other hand, the presence of Al octahedral coordination in Roman concrete is significantly low (supplementary Fig. S.2), even though it also contains hydrocalumite and ettringite (Jackson et al., 2012). These discrepancies between the developed calcined clay-portlandite system and Roman concrete, including formation of higher amounts of ettringite, hydrocalumite, and formation of geopolymer gel, are attributed to the relatively higher amounts of Al present in calcined clay. The chemical composition of the volcanic ash used in the production of Roman concrete is not well known yet. However, based on the general composition database (Vogel et al., 2017), volcanic ash contains around 13 to 19% Al_2O_3, which is lower than the Al_2O_3 present in the clay samples (Table 1). A higher Al content may have resulted a faster reaction rate of calcined clays compared to that of volcanic ash, considering the presence of Al enhances the reactivity of amorphous aluminosilicates by weakening the network due to the lower bond strength of Al-O-Si compared to that of the Si-O-Si (Amilton et al., 2001; Scholer et al., 2017; Nie et al., 2020). The high Al content of calcined clay can also be considered beneficial, allowing the recreated system to achieve higher mechanical strength. Although the compressive strengths of ancient Roman concrete varies depending on the types of aggregate, installation technique, and proportions (Jackson et al., 2009a), the average reported compressive strength of the Roman concrete is around 6 MPa (Giavarini et al., 2006; Jackson et al., 2009b). The direct comparison of the strength of Roman 'concrete' with the produced 'paste' samples may not be fair as the former one contained porous aggregates (volcanic tuffs, pumice). Nevertheless, the recreated system appears to provide higher strength (25 MPa) than the ancient Roman concrete.

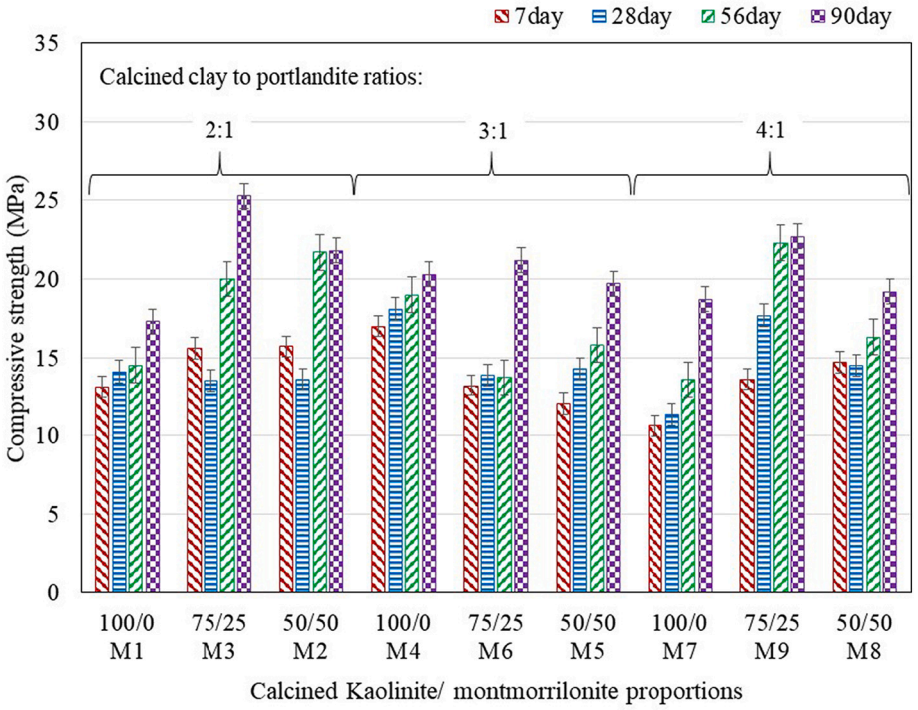

Fig. 11. Compressive strengths of calcined clay-portlandite paste samples.

5. Conclusion

The followings are the concluding remarks of the presented work:

(i) The primary microstructural phases in the calcined clay and portlandite systems cured in seawater include phillipsite, hydrocalumite, C-A-S-H, and ettringite which are also commonly found in Roman concrete.
(ii) Calcined clay-portlandite paste produced using clay blends containing around 50 to 75% by weight of calcined Kaol showed faster reaction rate and superior mechanical performance compared to those containing 100% calcined Kaol. Therefore, natural Kaol clay with a certain level of impurities can be used for the developed system.
(iii) Mineralization of ions (chlorides and sulfates) present in seawater, especially the formation of hydrocalumite, was identified as one of the primary factors contributing to the compressive strength development of the calcined-portlandite mixtures. By comparing with previously published studies (Boonjaeng et al., 2014), it was observed that the calcined clay-portlandite mixture prepared with seawater provided higher strength than those prepared using a NaOH solution (0.01 M to 10 M), hence indicating the significant role of seawater ions in the performance development of the calcined clay-portlandite systems.
(iv) Due to the relatively high Al content of calcined clay, the recreated system was found to have geopolymer gel formation, which was not present in Roman concrete. Regardless, the high Al content also resulted in a faster reaction rate and higher strength of the recreated system, therefore making it more appropriate for modern applications.

This article primarily focused on understanding the mechanical performance and reaction mechanism of the developed binder system. The durability performances of the developed Roman-inspired binders will be investigated in the future studies.

CRediT authorship contribution statement

Warda Ashraf: Conceptualization, Formal analysis, Investigation, Funding acquisition, Supervision, Writing – review & editing. **Ishrat Baki Borno:** Data curation, Formal analysis, Investigation. **Rakibul I. Khan:** Data curation, Formal analysis, Investigation. **Salman Siddique:** Data curation, Formal analysis, Investigation. **Muhammad Intesarul Haque:** Data curation, Formal analysis, Investigation. **Adhora Tahsin:** Data curation, Formal analysis, Investigation.

Declaration of Competing Interest

The authors declare that no conflict of interest is involved in this paper and the authors are responsible for the content and writing.

Data availability

Data will be made available on request.

Acknowledgement

This work was conducted with the funding support from the US Defense Advanced Research Projects Agency (DARPA, award #W911NF2010308) at the University of Texas at Arlington. All opinions, findings, and conclusions or recommendations expressed in this material are those of the authors and do not necessarily reflect the views of the sponsor. Dr. Andre Sutrisno, NMR Spectroscopist, School of Chemical Sciences, University of Illinois at Urbana-Champaign is gratefully acknowledged for his help and guidance regarding the NMR measurements presented in this article.

Appendix A. Supplementary data

Supplementary data to this article can be found online at https://doi.org/10.1016/j.clay.2022.106696.

References

Ababneh, A., Matalkah, F., Matalkeh, B., 2022. Effects of kaolin characteristics on the mechanical properties of alkali-activated binders. Constr. Build. Mater. 318 https://doi.org/10.1016/j.conbuildmat.2021.126020.

Alberto, Franco, Sommariva, Zunino, 2020. Limestone calcined clay cements (LC3): Raw material processing, sulfate balance and hydration kinetics. In: Ecole Polytechnique Fédérale de Lausanne.

Alonso, S., Palomo, A., 2001a. Alkaline activation of metakaolin and calcium hydroxide mixtures: influence of temperature, activator concentration and solids ratio. Mater. Lett. 47 (1–2), 55–62.

Alonso, Santiago, Palomo, A., 2001b. Calorimetric study of alkaline activation of calcium hydroxide ± metakaolin solid mixtures. Cem. Concr. Res. 31.

Amilton, J.A.P.H., Rantley, S.U.L.B., Antano, C.A.G.P., Riscenti, L.O.J.C., Ubicki, J.A.D. K., 2001. Dissolution of nepheline, jadeite and albite glasses: toward better models for aluminosilicate dissolution. Geochim. Cosmochim. Acta 65, 3683–3702.

Ashraf, W., 2018. Microstructure of chemically activated of gamma-dicalcium silicate paste. Constr. Build. Mater. 185, 617–627. https://doi.org/10.1016/j.conbuildmat.2018.07.030.

Boonjaeng, S., Chindaprasirt, P., Pimraksa, K., 2014. Lime-calcined clay materials with alkaline activation: phase development and reaction transition zone. Appl. Clay Sci. 95, 357–364. https://doi.org/10.1016/j.clay.2014.05.002.

Chen, X., Sutrisno, A., Struble, L.J., 2018. Effects of calcium on setting mechanism of metakaolin-based geopolymer. J. Am. Ceram. Soc. 101, 957–968. https://doi.org/10.1111/jace.15249.

Cole, W.F., Lancucki, C.J., 1983. Products formed in an aged concrete the occurrence of okenite. Cem. Concr. Res. 13, 611–618. https://doi.org/10.1016/0008-8846(83)90049-2.

Deboucha, W., Leklou, N., Khelidj, A., Oudjit, M.N., 2017. Hydration development of mineral additives blended cement using thermogravimetric analysis (TGA): Methodology of calculating the degree of hydration. Constr. Build. Mater. 146, 687–701. https://doi.org/10.1016/j.conbuildmat.2017.04.132.

Dhandapani, Y., Santhanam, M., 2020. Investigation on the microstructure-related characteristics to elucidate performance of composite cement with limestone-calcined clay combination. Cem. Concr. Res. 129 https://doi.org/10.1016/j.cemconres.2019.105959.

Du, H., Pang, S.D., 2020. High-performance concrete incorporating calcined kaolin clay and limestone as cement substitute. Constr. Build. Mater. 264 https://doi.org/10.1016/j.conbuildmat.2020.120152.

Duxson, P., Fernández-Jiménez, A., Provis, J.L., Lukey, G.C., Palomo, A., Van Deventer, J.S.J., 2007. Geopolymer technology: the current state of the art. J. Mater. Sci. 42, 2917–2933. https://doi.org/10.1007/s10853-006-0637-z.

Faucon, P., Charpentier, T., Bertrandie, D., Nonat, A., Virlet, J., Petit, J.C., Mirande, S., January, R.V., 1998. Characterization of calcium aluminate hydrates and related hydrates of cement pastes by 27 Al MQ-MAS NMR. Inorg. Chem. 37, 3726–3733.

Fernandez, R., Martirena, F., Scrivener, K.L., 2011. The origin of the pozzolanic activity of calcined clay minerals: a comparison between kaolinite, illite and montmorillonite. Cem. Concr. Res. 41, 113–122. https://doi.org/10.1016/j.cemconres.2010.09.013.

Frías, M., Vigil de la Villa, R., Martínez-Ramírez, S., García-Giménez, R., Sánchez de Rojas, M.I., 2020. Mineral phases in metakaolin-portlandite pastes cured 15 years at 60 °C. New data for scientific advancement. Appl. Clay Sci. 184. https://doi.org/10.1016/j.clay.2019.105368.

Gao, X., Yu, Q.L., Brouwers, H.J.H., 2017. Apply 29Si, 27Al MAS NMR and selective dissolution in identifying the reaction degree of alkali activated slag-fly ash composites. Ceram. Int. 43, 12408–12419. https://doi.org/10.1016/j.ceramint.2017.06.108.

Garcia-Lodeiro, I., Fernandez-Jimenez, A., Palomo, A., 2013. Hydration kinetics in hybrid binders: early reaction stages. Cem. Concr. Compos. 39, 82–92. https://doi.org/10.1016/j.cemconcomp.2013.03.025.

Garg, N., Skibsted, J., 2019. Dissolution kinetics of calcined kaolinite and montmorillonite in alkaline conditions: evidence for reactive Al(V) sites. J. Am. Ceram. Soc. 102, 7720–7734. https://doi.org/10.1111/jace.16663.

Gevers, B.R., Labuschagné, F.J.W.J., 2020. Green synthesis of hydrocalumite (CaAl-OH-LDH) from Ca(OH) 2 and Al(OH) 3 and the parameters that influence its formation and speciation. Crystals (Basel) 1, 1–26. https://doi.org/10.3390/cryst10080672.

Giavarini, C., Ferretti, Alessandro Samuelli, Santarelli, M.L., 2006. Mechanical characteristics of Roman "Opus Caementicium,". In: Kourkoulis, S.K. (Ed.), Fracture and Failure of Natural Building Stones: Applications in the Restoration of Ancient Monuments.

Gotti, E., Oleson, J.P., Bottalico, L., Brandon, C., Cucitore, R., Hohlfelder, R.L., 2008. A comparison of the chemical and engineering characteristics of ancient roman hydraulic concrete with a modern reproduction of vitruvian hydraulic concrete. Archaeometry 50, 576–590. https://doi.org/10.1111/j.1475-4754.2007.00371.x.

Granizo, M.L., Alonso, S., Blanco-varela, M.T., Palomo, A., 2002. Alkaline Activation of Metakaolin: Effect of Calcium Hydroxide in the Products of Reaction, 31, pp. 225–231.

Habert, G., Ouellet-plamondon, C., 2016. Recent update on the environmental impact of geopolymers. RILEM Techn. Lett. 1, 17–23.

Hernandez, J.F.M., Middendorf, B., Gehrke, M., Budelmann, H., 1998. Use of wastes of the sugar industry as pozzolana in lime-pozzolana binders: Study of the reaction. Cem. Concr. Res. 28, 1525–1536.

Hewlett, P., Liska, M. (Eds.), 2019. Lea's Chemistry of Cement and Concrete by Peter Hewlett. Butterworth-Heinemann. https://doi.org/10.1016/B978-0-7506-6256-7.50031-X.

Jackson, M.D., Logan, J.M., Scheetz, B.E., Deocampo, D.M., Cawood, C.G., Marra, F., Vitti, M., Ungaro, L., 2009a. Assessment of material characteristics of ancient concretes, Grande Aula, Markets of Trajan, Rome. J. Archaeol. Sci. 36, 2481–2492. https://doi.org/10.1016/j.jas.2009.07.011.

Jackson, M.D., Logan, J.M., Scheetz, B.E., Deocampo, D.M., Cawood, C.G., Marra, F., Vitti, M., Ungaro, L., 2009b. Assessment of material characteristics of ancient concretes, Grande Aula, Markets of Trajan, Rome. J. Archaeol. Sci. 36, 2481–2492. https://doi.org/10.1016/j.jas.2009.07.011.

Jackson, Marie D., Vola, G., Všianský, D., Oleson, J.P., Scheetz, B.E., Brandon, C., Hohlfelder, R.L., 2012. Cement microstructures and durability in ancient roman seawater concretes. In: Historic Mortars: Characterisation, Assessment and Repair, RILEM Bookseries, 7, pp. 49–76. https://doi.org/10.1007/978-94-007-4635-0.

Jackson, Marie D., Chae, S.R., Mulcahy, S.R., Meral, C., Taylor, R., Li, P., Emwas, A.H., Moon, J., Yoon, S., Vola, G., Wenk, H.R., Monteiro, P.J.M., 2012a. Unlocking the secrets of Al-tobermorite in Roman seawater concrete. Am. Mineral. 98, 1669–1687. https://doi.org/10.2138/am.2013.4484.

Jackson, Marie D., Chae, S.R., Mulcahy, S.R., Meral, C., Taylor, R., Li, P., Emwas, A.H., Moon, J., Yoon, S., Vola, G., Wenk, H.R., Monteiro, P.J.M., 2012b. Unlocking the secrets of Al-tobermorite in Roman seawater concrete. Am. Mineral. 98, 1669–1687. https://doi.org/10.2138/am.2013.4484.

Jackson, M.D., Moon, J., Gotti, E., Taylor, R., Chae, S.R., Kunz, M., Emwas, A.H., Meral, C., Guttmann, P., Levitz, P., Wenk, H.R., Monteiro, P.J.M., 2013. Material and elastic properties of Al-tobermorite in ancient roman seawater concrete. J. Am. Ceram. Soc. 96, 2598–2606. https://doi.org/10.1111/jace.12407.

Jackson, M.D., Landis, E.N., Brune, P.F., Vitti, M., Chen, H., Li, Q., Kunz, M., Wenk, H.R., Monteiro, P.J.M., Ingraffea, A.R., 2014. Mechanical resilience and cementitious processes in Imperial Roman architectural mortar. Proc. Natl. Acad. Sci. U. S. A. 111, 18484–18489. https://doi.org/10.1073/pnas.1417456111.

Jackson, M.D., Mulcahy, S.R., Chen, H., Li, Y., Li, Q., Cappelletti, P., Wenk, H.R., 2017. Phillipsite and Al-tobermorite mineral cements produced through low-temperature water-rock reactions in Roman marine concrete. Am. Mineral. 102, 1435–1450. https://doi.org/10.2138/am-2017-5993CCBY.

Jackson, M.D., Oleson, J.P., Moon, J., Zhang, Y., Chen, H., Gudmundsson, M.T., 2018. Extreme durability in ancient Roman concretes. Am. Ceram. Soc. Bull. 97, 22–28.

Juenger, M.C.G., Siddique, R., 2015. Recent advances in understanding the role of supplementary cementitious materials in concrete. Cem. Concr. Res. 78, 71–80. https://doi.org/10.1016/j.cemconres.2015.03.018.

Juenger, M.C.G., Snellings, R., Bernal, S.A., 2019. Supplementary cementitious materials: new sources, characterization, and performance insights. Cem. Concr. Res. 122, 257–273. https://doi.org/10.1016/j.cemconres.2019.05.008.

Khalifa, A.Z., Cizer, Ö., Pontikes, Y., Heath, A., Patureau, P., Bernal, S.A., Marsh, A.T.M., 2020. Advances in alkali-activation of clay minerals. Cem. Concr. Res. 132, 106050 https://doi.org/10.1016/j.cemconres.2020.106050.

Kobera, L., Brus, J., Klein, P., Dedecek, J., Urbanova, M., 2014. Biaxial Q-shearing of 27 Al 3QMAS NMR spectra: insight into the structural disorder of framework aluminosilicates. Solid State Nucl. Magn. Reson. 57–58, 29–38. https://doi.org/10.1016/j.ssnmr.2013.11.003.

Krishnan, S., Emmanuel, A.C., Bishnoi, S., 2019. Hydration and phase assemblage of ternary cements with calcined clay and limestone. Constr. Build. Mater. 222, 64–72. https://doi.org/10.1016/j.conbuildmat.2019.06.123.

Leroux, F., Philippe, L., Rousselot, I., Taviot-gu, C., Palvadeau, P., Besse, J., 2002. Insights on the structural chemistry of hydrocalumite and hydrotalcite-like materials: investigation of the series by X-Ray powder diffraction. J. Solid State Chem. 167, 137–144. https://doi.org/10.1006/jssc.2002.9635.

Li, Q., Geng, H., Shui, Z., Huang, Y., 2015. Effect of metakaolin addition and seawater mixing on the properties and hydration of concrete. Appl. Clay Sci. 115, 51–60. https://doi.org/10.1016/j.clay.2015.06.043.

Lin, H., Liu, H., Li, Y., Kong, X., 2021. Properties and reaction mechanism of phosphoric acid activated metakaolin geopolymer at varied curing temperatures. Cem. Concr. Res. 144 https://doi.org/10.1016/j.cemconres.2021.106425.

Macfarlane, J., Vanorio, T., Monteiro, P.J.M., 2021. Multi-scale imaging, strength and permeability measurements: Understanding the durability of Roman marine concrete. Constr. Build. Mater. 272, 121812 https://doi.org/10.1016/j.conbuildmat.2020.121812.

Maier, M., Beuntner, N., Thienel, K.C., 2021. Mineralogical characterization and reactivity test of common clays suitable as supplementary cementitious material. Appl. Clay Sci. 202 https://doi.org/10.1016/j.clay.2021.105990.

Maragh, J.M., Weaver, J.C., Masic, A., 2019. Large-scale micron-order 3D surface correlative chemical imaging of ancient Roman concrete. PLoS One 14, 2130–2132. https://doi.org/10.1371/journal.pone.0210710.

Massazza, F., 1993. Pozzolanic Cements. Cem. Concr. Compos. 15, 185–214.

Mccarthy, M.J., Dyer, T.D., 2019. Pozzolanas and pozzolanic materials. In: Lea's Chemistry of Cement and Concrete, 5th ed. Elsevier Ltd. https://doi.org/10.1016/B978-0-08-100773-0.00009-5

Miller, S.A., Horvath, A., Monteiro, P.J.M., 2018. Impacts of booming concrete production on water resources worldwide. Nat. Sustain. 1, 69–76. https://doi.org/10.1038/s41893-017-0009-5.

Monteiro, P.J.M., Miller, S.A., Horvath, A., 2017. Towards sustainable concrete. Nat. Mater. 16, 698–699. https://doi.org/10.1038/nmat4930.

Nie, S., Thomsen, R.M., Skibsted, J., 2020. Impact of Mg substitution on the structure and pozzolanic reactivity of calcium aluminosilicate (CaO-Al 2 O 3 -SiO 2) glasses. Cem. Concr. Res. 138, 106231 https://doi.org/10.1016/j.cemconres.2020.106231.

Oleson, J.P., Bottalico, L., Brandon, C., Cucitore, R., Gotti, E., Hohlfelder, R.L., 2006. Reproducing a Roman Maritime structure with Vitruvian pozzolanic concrete. J. Roman Archaeol. 19, 29–52. https://doi.org/10.1017/S1047759400006255.

Palomo, A., Monteiro, P., Martauz, P., Bilek, V., Fernandez-Jimenez, A., 2019. Hybrid binders: a journey from the past to a sustainable future (opus caementicium futurum). Cem. Concr. Res. 124, 105829 https://doi.org/10.1016/j.cemconres.2019.105829.

Pollio, V., 1914. The Ten Books on Architecture. Hathitrust.

Provis, J.L., Bernal, S.A., 2014. Geopolymers and Related Alkali-Activated Materials. Annu. Rev. Mater. Res. 44, 299–327. https://doi.org/10.1146/annurev-matsci-070813-113515.

Puligilla, S., Mondal, P., 2015. Co-existence of aluminosilicate and calcium silicate gel characterized through selective dissolution and FTIR spectral subtraction. Cem. Concr. Res. 70, 39–49. https://doi.org/10.1016/j.cemconres.2015.01.006.

Rajabipour, F., Giannini, E., Dunant, C., Ideker, J.H., Thomas, M.D.A., 2015. Alkali-silica reaction: current understanding of the reaction mechanisms and the knowledge gaps. Cem. Concr. Res. 76, 130–146. https://doi.org/10.1016/j.cemconres.2015.05.024.

Rhodes, C.J., 2018. Roman concrete for durable, eco-friendly construction – applications for tidal power generation, and protection against sea level rise CHRISTOPHER. Sci. Prog. 101, 83–91.

Santhanam, M., Cohen, M., Olek, J., 2006. Differentiating seawater and groundwater sulfate attack in Portland cement mortars. Cem. Concr. Res. 36, 2132–2137. https://doi.org/10.1016/j.cemconres.2006.09.011.

Scholer, A., Winnefeld, F., Haha, M. Ben, Lothenbach, B., 2017. The effect of glass composition on the reactivity of synthetic glasses. J. Am. Ceram. Soc. 100, 2253–2567. https://doi.org/10.1111/jace.14759.

Scrivener, K.L., John, V.M., Gartner, E.M., 2018. Eco-efficient cements: potential economically viable solutions for a low-CO2 cement-based materials industry. Cem. Concr. Res. 114, 2–26. https://doi.org/10.1016/j.cemconres.2018.03.015.

Scrivener, K., Martirena, F., Bishnoi, S., Maity, S., 2018a. Calcined clay limestone cements (LC3). Cem. Concr. Res. 114, 49–56. https://doi.org/10.1016/j.cemconres.2017.08.017.

Scrivener, K., Snellings, R., Lothenbach, B., 2018b. A Practical Guide to Microstructural Analysis of Cementitious Materials. CRC Press.

Sevelsted, T.F., Skibsted, J., 2015. Carbonation of C–S–H and C–A–S–H samples studied by 13C, 27Al and 29Si MAS NMR spectroscopy. Cem. Concr. Res. 71, 56–65. https://doi.org/10.1016/j.cemconres.2015.01.019.

Shah, V., Parashar, A., Scott, A., 2022. Understanding the importance of carbonates on the performance of Portland metakaolin cement. Constr. Build. Mater. 319 https://doi.org/10.1016/j.conbuildmat.2021.126155.

Skibsted, J., Henderson, E., Jakobsen, H.J., 1993. Characterization of Calcium Alumínate phases in cements by 27A1 MAS NMR spectroscopy. Inorg. Chem. 32, 1013–1027.

Slaty, F., Khoury, H., Wastiels, J., Rahier, H., 2013. Characterization of alkali activated kaolinitic clay. Appl. Clay Sci. 75–76, 120–125. https://doi.org/10.1016/j.clay.2013.02.005.

Tironi, A., Trezza, M.A., Scian, A.N., Irassar, E.F., 2012. Kaolinitic calcined clays: Factors affecting its performance as pozzolans. Constr. Build. Mater. 28, 276–281. https://doi.org/10.1016/j.conbuildmat.2011.08.064.

Vanorio, T., Kanitpanyacharoen, W., 2015. Rock physics of fibrous rocks akin to Roman concrete explains uplifts at Campi Flegrei Caldera. Science 1979 (349), 617–622.

Vejmelková, E., Keppert, M., Rovnaníková, P., Ondrác, M., Robert, C., 2012. Cement & Concrete Composites Properties of High Performance Concrete Containing Fine-Ground Ceramics as Supplementary Cementitious Material, 34, pp. 55–61. https://doi.org/10.1016/j.cemconcomp.2011.09.018.

Villain, G., Thiery, M., Platret, G., 2007. Measurement methods of carbonation profiles in concrete: thermogravimetry, chemical analysis and gammadensimetry. Cem. Concr. Res. 37, 1182–1192. https://doi.org/10.1016/j.cemconres.2007.04.015.

Vogel, A., Diplas, S., Durant, A.J., Azar, A.S., Sunding, M.F., Rose, W.I., Bonadonna, C., Krüger, K., 2017. Reference data set of volcanic ash physicochemical and optical properties. J. Geophys. Res.-Atmos. 9485–9514 https://doi.org/10.1002/2016JD026328.

Walkley, B., Provis, J.L., 2019. Solid-state nuclear magnetic resonance spectroscopy of cements. Mater Today Adv 1, 100007. https://doi.org/10.1016/j.mtadv.2019.100007.

Wang, S.D., Scrivener, K.L., 2003. 29Si and 27Al NMR study of alkali-activated slag. Cem. Concr. Res. 33, 769–774. https://doi.org/10.1016/S0008-8846(02)01044-X.

Weems, J.B., 2022. Chemistry of Clays.

Yi, Y., Zhu, D., Guo, S., Zhang, Z., Shi, C., 2020. A review on the deterioration and approaches to enhance the durability of concrete in the marine environment. Cem. Concr. Compos. 113, 103695 https://doi.org/10.1016/j.cemconcomp.2020.103695.

Yip, C.K., Lukey, G.C., Van Deventer, J.S.J., 2005. The coexistence of geopolymeric gel and calcium silicate hydrate at the early stage of alkaline activation. Cem. Concr. Res. 35, 1688–1697. https://doi.org/10.1016/j.cemconres.2004.10.042.

Yip, C.K., Lukey, G.C., Provis, J.L., Van Deventer, J.S.J., 2008. Effect of Calcium Silicate Sources on Geopolymerisation, 38, pp. 554–564. https://doi.org/10.1016/j.cemconres.2007.11.001.

Yunsheng, Z., Wei, S., Zongjin, L., 2010. Composition design and microstructural characterization of calcined kaolin-based geopolymer cement. Appl. Clay Sci. 47, 271–275. https://doi.org/10.1016/j.clay.2009.11.002.

Zhang, B., Guo, H., Yuan, P., Li, Y., Wang, Q., Deng, L., Liu, D., 2020. Geopolymerization of halloysite via alkali-activation: Dependence of microstructures on precalcination. Appl. Clay Sci. 185 https://doi.org/10.1016/j.clay.2019.105375.